

THE SPREAD OF METALS INTO THE LOW-REDSHIFT INTERGALACTIC MEDIUM

CAMERON T. PRATT,¹ JOHN T. STOCKE,¹ BRIAN A. KEENEY,¹ AND CHARLES W. DANFORTH¹

¹*Center for Astrophysics and Space Astronomy, Department of Astrophysical and Planetary Sciences, University of Colorado, 389 UCB, Boulder, CO 80309, USA*

ABSTRACT

We investigate the association between galaxies and metal-enriched and metal-deficient absorbers in the local universe ($z < 0.16$) using a large compilation of FUV spectra of bright AGN targets observed with the Cosmic Origins Spectrograph aboard the *Hubble Space Telescope*. In this homogeneous sample of 18 O VI detections at $N_{\text{O VI}} \geq 13.5 \text{ cm}^{-2}$ and 18 non-detections at $N_{\text{O VI}} < 13.5 \text{ cm}^{-2}$ using Ly α absorbers with $N_{\text{HI}} \geq 10^{14} \text{ cm}^{-2}$, the maximum distance O VI extends from galaxies of various luminosities is ~ 0.6 Mpc, or ~ 5 virial radii, confirming and refining earlier results. This is an important value that must be matched by numerical simulations, which input the strength of galactic winds at the sub-grid level. We present evidence that the primary contributors to the spread of metals into the circum- and intergalactic media are sub- L^* galaxies ($0.25L^* < L < L^*$). The maximum distances that metals are transported from these galaxies is comparable to, or less than, the size of a group of galaxies. These results suggest that, where groups are present, the metals produced by the group galaxies do not leave the group. Since many O VI non-detections in our sample occur at comparably close impact parameters as the metal-bearing absorbers, some more pristine intergalactic material appears to be accreting onto groups where it can mix with metal-bearing clouds.

Keywords: quasars: absorption lines — galaxies: halos — intergalactic medium — galaxies: abundances — galaxies: evolution

1. INTRODUCTION

Models of galactic evolution must incorporate the accretion of low-metallicity gas ($Z \sim 0.1 Z_{\odot}$) from the ambient intergalactic medium (IGM; e.g., Oppenheimer et al. 2012) both in order to resolve the ‘‘G-dwarf problem’’ (Pagel 2009) and to maintain the high star formation rates seen in late-type galaxies like the Milky Way (Binney & Tremaine 1987). The modest metallicity of this accreting gas suggests a source within nearby, low-mass galaxies although the mass range of the source galaxies is not known specifically. Ultimately, a mixture of outflows and accretion composes the massive, gaseous halos that surround most late-type galaxies, known as the circumgalactic medium (CGM; Tumlinson et al. 2011; Stocke et al. 2013; Werk et al. 2014; Burchett et al. 2016; Keeney et al. 2017).

Some studies suggest that the CGM extends from the disk of a star-forming galaxy to its ‘‘virial radius’’ (R_{vir} ; Stocke et al. 2013; Shull 2014), which is the distance a galaxy has gravitational influence on its surroundings. At least one recent study presents evidence that the CGM does not extend much beyond $1/2 R_{\text{vir}}$ (Prochaska et al. 2017), but Shull (2014) argues that parts of the CGM can include unbound outflows beyond R_{vir} . Simulations suggest that the amount of gas and metals that escapes is a strong function of both galaxy mass and redshift, with ‘‘gusty’’ winds at high- z calming down to bound ‘‘galactic fountains’’ for the most massive halos at $z < 1$ (Muratov et al. 2015, 2017; Hayward & Hopkins 2017).

The boundary between the CGM and IGM is rather ambiguous, especially for galaxies of widely differing escape velocities. AGN absorption-line observations support this premise because there are no strong changes in H I absorber properties, including covering factor and mean H I column density, which decline monotonically in the $1\text{--}5 R_{\text{vir}}$ range (Stocke et al. 2013). However, metal-bearing absorbers decline rapidly away from the nearest galaxies (e.g., Chen et al. 1998; Finn et al. 2016; Burchett et al. 2016) and have yet to be detected in galaxy voids (Stocke et al. 2007).

Simulations by Oppenheimer et al. (2012) suggest that it is primarily low-mass galaxies whose supernova-driven winds enrich the IGM with metals, because winds produced by very massive galaxies ($M \geq 10^{11} M_{\odot}$) may be incapable of breaching their surrounding gaseous halos (Côté et al. 2012; Hayward & Hopkins 2017). Instead, these outflows may fall back onto galactic disks and re-ignite star formation (e.g., Veilleux, Cecil, & Bland-Hawthorn 2005), as in our own Galaxy (Keeney et al. 2006; Bordoloi et al. 2017).

When large-scale simulations (e.g., Davé et al. 1999, 2011; Cen & Ostriker 1999) place galactic winds in a cosmological context, the strength of these winds and their full range of extent often are input at a sub-pixel level (so-called sub-grid physics, but see recent, high-resolution simulations by the *FIRE* collaboration; Hopkins et al. 2016) so that the extent to which metals are transported away from their source galaxy is not determined *a priori* in most simulations. Thus, this maximum extent provides both an observational bound for a galaxy’s CGM and a constraint on galactic wind modeling within cosmological simulations.

In this paper, we estimate the maximum distance winds propagate away from galaxies using low-redshift absorption found in the far-ultraviolet (FUV) spectra of bright AGN obtained with the *Cosmic Origins Spectrograph* (COS) aboard the *Hubble Space Telescope* (*HST*), in conjunction with an extensive database of low- z galaxy positions and redshifts near these sight lines (Stocke et al. 2013; Keeney et al. 2017, B. Keeney et al. 2018, in preparation). Since O VI (1032, 1038 Å) exhibits the greatest extent away from galaxies of any of the ions detected in absorption in the FUV (Prochaska et al. 2011; Stocke et al. 2013; Keeney et al. 2017), this study uses only the O VI doublet.

The present O VI study expands upon and updates similar O VI work by Stocke et al. (2006), where a smaller sample of absorbers was used to determine that metals spread no more than ~ 800 kpc from L^* galaxies (see also Johnson, Chen, & Mulchaey 2015; Finn et al. 2016). For the remainder of this paper, Section 2 describes the absorption-line and galaxy survey data, Section 3 presents the results, and Section 4 provides a summary of our results and conclusions.

2. ABSORBER AND GALAXY SAMPLES

2.1. H I and O VI Absorber Sample

This search for galaxy-absorber associations uses the largest survey of the low- z IGM to date from Danforth et al. (2016). These authors used *HST*/COS FUV spectra to construct an absorber sample along 82 AGN sight lines in the redshift range $0.05 < z < 0.75$. The sample includes strong Ly α absorbers with $N_{\text{HI}} \geq 10^{14} \text{ cm}^{-2}$ from Danforth et al. (2016), although some H I column density measurements have been revised in Keeney et al. (2017) and this work. This limit is high enough that Ly β is detected for all these absorbers, increasing the accuracy of the N_{HI} measurement. Moreover, O VI (and Ly β) falls in the COS bandpass only at $z \gtrsim 0.11$. Since the galaxy redshift surveys employed are naturally weighted towards $z \leq 0.1$, previous data from the *Far-Ultraviolet Spectroscopic Explorer* (*FUSE*) satellite of a

few very bright AGN were incorporated to expand the range of coverage to more low- z O VI absorbers. The

strengths of absorbers used in this study are provided in [Table 1](#).

Table 1. Absorber Information

Sight Line	z_{abs}	$\log N_{\text{HI}}$ (cm^{-2})	Source	$\log N_{\text{OVI}}$ (cm^{-2})	Source
1ES 1028+511	0.14057	14.06 ± 0.18	Danforth et al. (2016)	<13.41	This Work
3C 263	0.06340	15.31 ± 0.19	This Work	14.52 ± 0.07	This Work
3C 263 *	0.11392	14.19 ± 0.12	Danforth et al. (2016)	13.65 ± 0.15	Danforth et al. (2016)
3C 263 *	0.12232	14.26 ± 0.08	Danforth et al. (2016)	<13.23	This Work
3C 263 *	0.14075	14.49 ± 0.06	Danforth et al. (2016)	13.73 ± 0.10	Danforth et al. (2016)
FBQS J1010+3003	0.12833	14.06 ± 0.32	Danforth et al. (2016)	<13.42	This Work
H 1821+643 *	0.12120	14.12 ± 0.03	Keeney et al. (2017)	<13.16	This Work
HE 0226-4110 *	0.06087	14.32 ± 0.10	This Work	<13.33	Tilton et al. (2012)
PG 0953+414 *	0.06809	14.52 ± 0.09	This Work	14.35 ± 0.11	Tilton et al. (2012)
PG 1001+291	0.11346	14.13 ± 0.19	Danforth et al. (2016)	<13.33	This Work
PG 1001+291 *	0.13744	15.22 ± 0.30	Danforth et al. (2016)	<13.27	This Work
PG 1048+342	0.14471	14.07 ± 0.16	Danforth et al. (2016)	<13.28	This Work
PG 1116+215	0.13853	15.95 ± 0.03	Keeney et al. (2017)	13.78 ± 0.02	Keeney et al. (2017)
PG 1216+069 A *	0.12375	14.57 ± 0.05	Keeney et al. (2017)	14.14 ± 0.06	Keeney et al. (2017)
PG 1216+069 B	0.12375	14.76 ± 0.05	Keeney et al. (2017)	14.12 ± 0.06	Keeney et al. (2017)
PG 1216+069 *	0.12478	14.74 ± 0.06	Danforth et al. (2016)	14.17 ± 0.15	Danforth et al. (2016)
PG 1216+069 *	0.13507	14.75 ± 0.07	Danforth et al. (2016)	<13.46	This Work
PG 1222+216 A *	0.15567	14.04 ± 0.10	Danforth et al. (2016)	<13.40	This Work
PG 1222+216 B *	0.15567	14.11 ± 0.06	Danforth et al. (2016)	<13.40	This Work
PG 1259+593	0.00763	14.05 ± 0.07	This Work	<13.30	This Work
PG 1259+593	0.04611	15.45 ± 0.04	Keeney et al. (2017)	13.94 ± 0.12	Keeney et al. (2017)
PG 1259+593	0.08935	14.11 ± 0.05	This Work	<13.04	This Work
PG 1424+240 *	0.12134	15.35 ± 0.29	Danforth et al. (2016)	14.52 ± 0.11	Danforth et al. (2016)
PG 1424+240 A *	0.14697	14.60 ± 0.06	Danforth et al. (2016)	13.87 ± 0.23	Danforth et al. (2016)
PG 1424+240 B	0.14697	15.58 ± 1.41	Danforth et al. (2016)	13.65 ± 0.23	Danforth et al. (2016)
PG 1626+554 *	0.09382	14.52 ± 0.53	This Work	<13.30	This Work
PHL 1811 *	0.07348	14.54 ± 0.15	This Work	<13.03	Tilton et al. (2012)
PHL 1811 *	0.07777	15.40 ± 0.07	Keeney et al. (2017)	<13.12	Keeney et al. (2017)
PHL 1811 A *	0.12060	14.42 ± 0.11	This Work	<13.14	This Work
PHL 1811 B *	0.12060	14.33 ± 0.22	Danforth et al. (2016)	<12.88	This Work
PHL 1811 *	0.13229	14.61 ± 0.01	Keeney et al. (2017)	13.88 ± 0.02	Keeney et al. (2017)
PHL 1811	0.13547	14.98 ± 0.13	Danforth et al. (2016)	13.54 ± 0.16	Danforth et al. (2016)

Table 1 continued

Table 1 (continued)

Sight Line	z_{abs}	$\log N_{\text{HI}}$ (cm^{-2})	Source	$\log N_{\text{OVI}}$ (cm^{-2})	Source
PKS 0405-123	0.09180	14.69 ± 0.03	This Work	13.83 ± 0.04	Tilton et al. (2012)
PKS 0405-123	0.09655	14.94 ± 0.02	This Work	13.71 ± 0.15	Tilton et al. (2012)
PKS 2005-489	0.01695	14.66 ± 0.19	This Work	13.76 ± 0.12	This Work
PKS 2005-489 *	0.06499	14.10 ± 0.22	This Work	13.61 ± 0.07	Tilton et al. (2012)
Q 1230+0115 *	0.07807	15.11 ± 0.53	This Work	14.47 ± 0.37	This Work
SBS 1122+594	0.14315	14.33 ± 0.26	Danforth et al. (2016)	<13.47	This Work
SBS 1122+594	0.15545	15.11 ± 0.21	Danforth et al. (2016)	14.10 ± 0.09	Danforth et al. (2016)
TON 580	0.13396	14.31 ± 0.15	Danforth et al. (2016)	<13.47	This Work

^{A/B}Two partially blended absorbers that are treated as a single system.

*Absorbers included in the “matched” N_{HI} subsamples.

Only “clean” detections and non-detections of O VI were utilized; meaning, the spectra exhibit no intervening lines (e.g. interstellar transitions or redshifted Ly α lines) at the same wavelengths of O VI. Also, the O VI doublet is required to be sampled at high signal-to-noise ($S/N > 15$), allowing the $\geq 3\sigma$ detection of O VI at $N_{\text{OVI}} \gtrsim 10^{13.5} \text{ cm}^{-2}$, or upper limits below that level. The median value for the 18 O VI detections is $N_{\text{OVI}} = 10^{13.9} \text{ cm}^{-2}$ while all the 18 non-detections are at $N_{\text{OVI}} < 10^{13.5} \text{ cm}^{-2}$.

Additionally, to permit counting only one absorber-galaxy correlation per galaxy halo, we treated any O VI absorptions with $|\Delta v| < 250 \text{ km s}^{-1}$ as a single system in the same halo (see discussion of absorber systems in Stocke et al. 2014). While the S/N of the COS FUV spectra is not uniform, these high-S/N data allow a median detection of metal-enriched absorbers at the $\sim 10\%$ solar level; although, some metallicities in the sample may be as low as a few percent solar values based on the analysis of similar absorbers by Savage et al. (2014). Starting with a Ly α absorption-line redshift, there were 18 detections and 18 non-detections in O VI at $z < 0.16$.

The “full” samples of absorbers were created using all of the available high-S/N spectra in the Danforth et al. (2016) compilation. It was determined, however, that the O VI non-detections have systematically smaller N_{HI} values than the detections. In order to check for potential biases caused by this difference, we constructed “matched” subsamples of O VI detections and non-detections by matching their N_{HI} values within 0.2 dex for each pair. By this process, 10 matched pairs in N_{HI} (indicated by asterisks in Table 1) were created so that two subsamples could be drawn from the same parent population in N_{HI} (Anderson-Darling p -value =

0.99). It was not possible to obtain a larger matched sample due to the very strong correlation between N_{HI} and impact parameter to the nearest galaxy, which has been known since the seminal work of Lanzetta et al. (1995) and is almost certainly a consequence of large-scale structure formation (Davé et al. 1999). In Section 3, results are presented using both the full samples and these samples of matched pairs.

Danforth et al. (2016) and Keeney et al. (2017) list the absorbers used in this survey and provide spectra, velocities and equivalent widths or limits for H I and common metal-line species, including C II, C III, C IV, Si II, Si III, Si IV, and O VI, when they occur within the *HST*/COS or *FUSE* bandpasses. Since all of these absorbers include at least H I Ly α , absorber velocities for Ly α are used and have a velocity error of $\pm 15 \text{ km s}^{-1}$ due to the absolute wavelength uncertainty of the *HST*/COS G130M and G160M gratings (Green et al. 2012). Somewhat larger velocity errors are quoted for some absorbers in Danforth et al. (2016) and Keeney et al. (2017) for Ly α lines with complex line profiles.

2.2. Galaxy Redshift Surveys

The galaxy data were obtained from four ground-based telescopes: the Sloan Digital Sky Survey (SDSS) spectroscopic sample (DR12; Alam et al. 2015) and multi-object spectroscopy (MOS) from the 3.5-m Wisconsin-Indiana-Yale-NOAO (WIYN) telescope at Kitt Peak National Observatory, the 3.9-m Anglo-Australian Telescope (AAT), and the 4-m Blanco telescope at Cerro Tololo Inter-American Observatory. While the SDSS spectroscopic survey is relatively shallow ($m_r \leq 17.8$), it provides large-angle coverage which is unmatched in the south, where we relied upon a compilation of various galaxy redshift surveys including the

2dF (Colless et al. 2007) and 6dF (Jones et al. 2009) surveys. These wide-field surveys were complemented by much deeper ($m_g \leq 20$) MOS, primarily obtained at WIYN with the HYDRA spectrograph. Individual field completeness levels vary but are typically $> 90\%$ out to completeness impact parameters (ρ_{lim}) of 0.5-2 Mpc for most absorbers; details of the observational process, data reduction and analysis, and redshift determination are presented in B. Keeney et al. (2018, in preparation).

There are several reasons why the completeness for obtaining measurable redshifts does not reach 100%, including an inability to place fibers on galaxies separated by $\leq 20''$ on the sky, and very diffuse galaxies whose spectrum is inconclusive despite a total magnitude brighter than a given completeness limit (L_{lim}) at the absorber redshift.

Table 2 presents the completeness levels of our galaxy surveys for each absorber. A completeness level $\geq 90\%$ is required herein as in our first study Stocke et al. (2006). Blank entries are not complete to L_{lim} at $\geq 90\%$, and so are not part of this survey. Absorbers with entries of “SDSS” are complete to $\geq 94\%$ based on the limits of DR12 (see Alam et al. 2015, B. Keeney et al. 2018, in preparation). Some of the luminosities in Table 3 differ somewhat from those presented in Stocke et al. (2014) because they have been updated using our own photometry and analysis procedure (see detailed discussion in Keeney et al. 2017) compared to earlier results from the literature (e.g., Prochaska et al. 2011).

2.3. Nearest Galaxy Data

Although redshift accuracies vary somewhat depending on the intrinsic galaxy spectrum (e.g., pure emission-line, emission plus absorption line, or pure absorption line), these errors are typically $\pm 30 \text{ km s}^{-1}$ as determined for objects that were observed multiple times in our program (B. Keeney et al. 2018, in preparation). We *de facto* assume that any galaxy within $\pm 1000 \text{ km s}^{-1}$ of the absorber velocity could be associated with the absorber, but compute a three-dimensional distance between each of these nearby galaxies and the absorbers by assuming a “reduced Hubble flow” model. Under this assumption, the line-of-sight distance between absorbers and galaxies (D_{los}) is zero where the galaxy-absorber velocity difference, $|\Delta v| \leq 400 \text{ km s}^{-1}$ and is otherwise determined using “pure Hubble flow”; i.e., $D_{\text{los}} = (|\Delta v| - 400 \text{ km s}^{-1})/H_0$.

While the “reduced velocity” limit is arbitrary, this choice is based upon the rotation speed of an $L > L^*$ galaxy plus an additional peculiar velocity to be conservative. Only a few galaxies with $|\Delta v| > 400 \text{ km s}^{-1}$ are

identified as nearest galaxies by this study, mostly for $L > L^*$ galaxies (6 cases).

We also consider scaled galaxy distances in units of R_{vir} . With rest-frame g -band luminosities for all galaxies, virial radii (and halo masses) are determined from their stellar mass using a halo-matching technique described in Stocke et al. (2013, see their Figure 1) and Keeney et al. (2017). Figure 1 of Stocke et al. (2013) shows the function adopted in comparison with different scaling relationships used by other groups. For $L > L^*$ galaxies, these virial radii are approximately a factor of two smaller than those assumed by Prochaska et al. (2011) or the COS-Halos team (e.g., Werk et al. 2014). Scrutiny of several dozen, low- z *HST*/COS-discovered absorbers finds that the identification of an absorber with a specific galaxy is robust out to $\rho \lesssim 1.4 R_{\text{vir}}$ (Keeney et al. 2017).

We identify individual galaxies as being “associated” with these absorbers, but it is possible that some absorbers are actually affiliated with entire groups of galaxies in which the nearest galaxy is a member of the group (discussed in detail in Stocke et al. 2014). Since virtually all galaxies are in groups of some size (see Local Supercluster studies by Tully et al. 2009), it is difficult to determine whether the absorber is most closely associated with an individual galaxy, particularly when $\rho \geq 1.4 R_{\text{vir}}$ (Keeney et al. 2017; see Stocke et al. 2017 for discussions of a specific case study). Moreover, there is no statistically meaningful way to discriminate between absorbers associated with groups vs. individual galaxies or to know which halo mass distribution these absorbers should be connected with. This is an ambiguity for all studies concerning absorber-galaxy connections at both low- and high- z (e.g., Steidel et al. 2010; Werk et al. 2014). Regardless, this study utilizes individual galaxy virial radii to estimate how far metals are spread from their putative source galaxy.

Table 3 presents the basic data used in this study, in which the third column identifies the O VI detections and non-detections. The remaining columns (keyed to the limiting galaxy luminosity, L_{lim}) list the nearest galaxy luminosity, L , and three-dimensional absorber-galaxy physical distance, D , and distances scaled by R_{vir} . Here we identify the nearest galaxy in two different ways: using the smallest physical distance and the smallest distance scaled by R_{vir} . Conceivably, it is possible for a very luminous galaxy to be the nearest galaxy to an absorber in terms of R_{vir} even if it is physically farther away than a lower-luminosity galaxy. Columns 4-7 use all available data regardless of galaxy luminosity. Columns 8-11, 12-15, and 16-19 use all galaxies with $L \geq 0.25 L^*$, $L \geq 0.5 L^*$, and $L \geq L^*$ respectively. Ab-

sorber regions that were not surveyed deeply enough to reach the limiting luminosities given at the top have no data shown.

Table 2. Galaxy Survey Completeness Limits Surrounding IGM Absorbers

Sight Line	z_{abs}	$L_{\text{lim}} = 0.25 L^*$		$L_{\text{lim}} = 0.5 L^*$		$L_{\text{lim}} = L^*$	
		ρ_{lim}	Completeness	ρ_{lim}	Completeness	ρ_{lim}	Completeness
		(Mpc)	(%)	(Mpc)	(%)	(Mpc)	(%)
1ES 1028+511	0.14057	3.00	100%	3.00	100%
3C 263	0.06340	1.48	100%	SDSS	SDSS	SDSS	SDSS
3C 263	0.11392	2.51	92.65%	2.51	100%	SDSS	SDSS
3C 263	0.12232	2.67	94.38%	2.67	100%	SDSS	SDSS
3C 263	0.14075	3.01	100%	3.01	100%
FBQS J1010+3003	0.12833	2.78	95.73%	2.78	100%	2.78	100%
H 1821+643	0.12120	2.65	93.07%	2.65	96.15%	SDSS	SDSS
HE 0226-4110	0.06087	1.42	100%	1.42	100%	1.42	100%
PG 0953+414	0.06809	1.58	100%	SDSS	SDSS	SDSS	SDSS
PG 1001+291	0.11346	2.50	94.87%	2.50	96.15%	SDSS	SDSS
PG 1001+291	0.13744	2.95	95.92%
PG 1048+342	0.14471	3.08	95%	2.00	100%
PG 1116+215	0.13853
PG 1216+069	0.12375	1.35	95.24%	2.16	92.86%	2.16	100%
PG 1216+069	0.12478	1.36	95.45%	2.17	93.33%	2.17	100%
PG 1216+069	0.13507	1.89	90.91%	2.32	100%
PG 1222+216	0.15567	2.78	100%
PG 1259+593	0.00763	SDSS	SDSS	SDSS	SDSS	SDSS	SDSS
PG 1259+593	0.04611	SDSS	SDSS	SDSS	SDSS	SDSS	SDSS
PG 1259+593	0.08935	2.02	91.43%	SDSS	SDSS
PG 1424+240	0.12134	2.65	95.45%	SDSS	SDSS
PG 1424+240	0.14697	2.65	93.55%	3.12	100%
PG 1626+554	0.09382	0.84	90.91%	0.84	100%	SDSS	SDSS
PHL 1811	0.07348	1.70	97.78%	1.70	100%	1.70	100%
PHL 1811	0.07777	1.78	98.11%	1.78	100%	1.78	100%
PHL 1811	0.12060	1.05	92.31%	2.64	98.65%	2.64	100%
PHL 1811	0.13229	1.14	92.59%	2.85	96.84%	2.85	100%
PHL 1811	0.13547	1.17	92.59%	2.91	96.94%	2.91	100%
PKS 0405-123	0.09180	1.87	100%	1.87	100%	1.87	100%
PKS 0405-123	0.09655	1.95	91.67%	1.95	100%	1.95	100%

Table 2 continued

Table 2 (*continued*)

Sight Line	z_{abs}	$L_{\text{lim}} = 0.25 L^*$		$L_{\text{lim}} = 0.5 L^*$		$L_{\text{lim}} = L^*$	
		ρ_{lim} (Mpc)	Completeness (%)	ρ_{lim} (Mpc)	Completeness (%)	ρ_{lim} (Mpc)	Completeness (%)
PKS 2005-489	0.01695
PKS 2005-489	0.06499	0.15	100%	0.15	100%	0.15	100%
Q 1230+0115	0.07807	1.79	100%	SDSS	SDSS	SDSS	SDSS
SBS 1122+594	0.14315	3.05	93.65%	1.52	100%
SBS 1122+594	0.15545	3.27	93.75%	2.94	92.31%
TON 580	0.13396	2.88	100%	2.88	100%	2.88	100%

Table 3. Distances from Absorbers to their Nearest Galaxies

Sight Line	z_{abs}	O VI	No Luminosity Limit						$L_{\text{lim}} = 0.25 L^*$						$L_{\text{lim}} = 0.5 L^*$						$L_{\text{lim}} = L^*$								
			Physical		Scaled by R_{vir}		Physical		Scaled by R_{vir}		Physical		Scaled by R_{vir}		Physical		Scaled by R_{vir}		Physical		Scaled by R_{vir}		Physical		Scaled by R_{vir}				
			L	D	L	D/R_{vir}	L	D	L	D/R_{vir}	L	D	L	D/R_{vir}	L	D	L	D/R_{vir}	L	D	L	D/R_{vir}	L	D	L	D/R_{vir}	L	D	L
IES 1028+511	0.14057	n	0.328	1.53	1.94	9.65	1.94	2.19	1.94	9.65	1.94	2.19	1.94	9.65	1.94	2.19	1.94	9.65	1.94	2.19	1.94	9.65	
3C 263	0.06340	y	0.283	0.064	0.283	0.538	0.283	0.064	0.283	0.538	0.283	0.538	0.283	0.064	0.283	0.538	0.283	0.064	0.283	0.538	0.283	0.064	0.283	0.538	0.283	0.064	0.283	0.538	
3C 263	0.11392	y	0.368	0.354	0.368	2.70	0.368	0.354	0.368	2.70	0.368	0.354	0.368	2.70	0.368	0.354	0.368	2.70	0.368	0.354	0.368	2.70	0.368	0.354	0.368	2.70	0.368	0.354	0.368
3C 263	0.12232	n	0.430	1.11	0.430	8.11	0.430	1.11	0.430	8.11	0.430	1.11	0.430	8.11	0.430	1.11	0.430	8.11	0.430	1.11	0.430	8.11	0.430	1.11	0.430	8.11	0.430	1.11	0.430
3C 263	0.14075	y	1.87	0.622	1.87	2.79	1.87	0.622	1.87	2.79	1.87	0.622	1.87	2.79	1.87	0.622	1.87	2.79	1.87	0.622	1.87	2.79	
FBQS J1010+3003	0.12833	n	0.235	0.529	1.49	3.18	1.49	0.658	1.49	3.18	1.49	0.658	1.49	3.18	1.49	0.658	1.49	3.18	1.49	0.658	1.49	3.18	1.49	0.658	1.49	3.18	1.49	0.658	
H 1821+643	0.12120	n	0.776	0.159	0.776	0.952	0.776	0.159	0.776	0.952	0.776	0.159	0.776	0.952	0.776	0.159	0.776	0.952	0.776	0.159	0.776	0.952	0.776	0.159	0.776	0.952	0.776	0.159	0.776
HE 0226-4110	0.06087	n	0.287	0.352	0.287	2.93	0.287	0.352	0.287	2.93	0.287	0.352	0.287	2.93	0.287	0.352	0.287	2.93	0.287	0.352	0.287	2.93	0.287	0.352	0.287	2.93	0.287	0.352	0.287
PG 0953+414	0.06809	y	0.892	0.611	0.892	3.49	0.892	0.611	0.892	3.49	0.892	0.611	0.892	3.49	0.892	0.611	0.892	3.49	0.892	0.611	0.892	3.49	0.892	0.611	0.892	3.49	0.892	0.611	0.892
PG 1001+291	0.11346	n	0.225	0.816	1.01	6.08	0.324	0.883	1.01	6.08	0.324	0.883	1.01	6.08	0.324	0.883	1.01	6.08	0.324	0.883	1.01	6.08	0.324	0.883	1.01	6.08	0.324	0.883	1.01
PG 1001+291	0.13744	n	0.132	0.055	0.132	0.585	0.132	0.055	0.132	0.585	0.132	0.055	0.132	0.585	0.132	0.055	0.132	0.585	0.132	0.055	0.132	0.585	
PG 1048+342	0.14471	n	0.364	0.410	0.364	3.15	0.364	0.410	0.364	3.15	0.364	0.410	0.364	3.15	0.364	0.410	0.364	3.15	0.364	0.410	0.364	3.15	
PG 1116+215	0.13853	y	1.76	0.139	1.76	0.632	1.76	0.139	1.76	0.632	1.76	0.139	1.76	0.632	1.76	0.139	1.76	0.632	1.76	0.139	1.76	0.632	
PG 1216+069	0.12375	y	0.657	0.094	0.657	0.595	0.657	0.094	0.657	0.595	0.657	0.094	0.657	0.595	0.657	0.094	0.657	0.595	0.657	0.094	0.657	0.595	0.657	0.094	0.657	0.595	0.657	0.094	0.657
PG 1216+069	0.12478	y	0.657	0.094	0.657	0.595	0.657	0.094	0.657	0.595	0.657	0.094	0.657	0.595	0.657	0.094	0.657	0.595	0.657	0.094	0.657	0.595	0.657	0.094	0.657	0.595	0.657	0.094	0.657
PG 1216+069	0.13507	n	1.38	0.758	1.38	3.75	1.38	0.758	1.38	3.75	1.38	0.758	1.38	3.75	1.38	0.758	1.38	3.75	1.38	0.758	1.38	3.75	
PG 1222+216	0.15567	n	0.646	0.498	0.646	3.17	0.646	0.498	0.646	3.17	0.646	0.498	0.646	3.17	0.646	0.498	0.646	3.17	0.646	0.498	0.646	3.17	
PG 1259+593	0.00763	n	0.085	0.474	0.770	3.51	0.770	0.586	0.770	3.51	0.770	0.586	0.770	3.51	0.770	0.586	0.770	3.51	0.770	0.586	0.770	3.51	0.770	0.586	0.770	3.51	0.770	0.586	0.770
PG 1259+593	0.04611	y	0.065	0.089	0.506	0.958	0.506	0.138	0.506	0.958	0.506	0.138	0.506	0.958	0.506	0.138	0.506	0.958	0.506	0.138	0.506	0.958	0.506	0.138	0.506	0.958	0.506	0.138	0.506
PG 1259+593	0.08935	n	0.198	1.76	0.429	12.9	0.429	1.76	0.429	12.9	0.429	1.76	0.429	12.9	0.429	1.76	0.429	12.9	0.429	1.76	0.429	12.9	0.429	1.76	0.429	12.9	0.429	1.76	0.429
PG 1424+240	0.12134	y	1.06	0.201	1.06	1.09	1.06	0.201	1.06	1.09	1.06	0.201	1.06	1.09	1.06	0.201	1.06	1.09	1.06	0.201	1.06	1.09	
PG 1424+240	0.14697	y	0.916	0.497	0.916	2.82	0.916	0.497	0.916	2.82	0.916	0.497	0.916	2.82	0.916	0.497	0.916	2.82	0.916	0.497	0.916	2.82	
PG 1626+554	0.09382	n	1.06	2.55	1.06	13.7	1.06	2.55	1.06	13.7	1.06	2.55	1.06	13.7	1.06	2.55	1.06	13.7	1.06	2.55	1.06	13.7	
PHL 1811	0.07348	n	0.131	0.344	2.97	1.95	0.620	0.446	2.97	1.95	0.620	0.446	2.97	1.95	0.620	0.446	2.97	1.95	0.620	0.446	2.97	1.95	0.620	0.446	2.97	1.95	0.620	0.446	2.97

Table 3 continued

Table 3 (continued)

Sight Line	z_{abs}	O VI	No Luminosity Limit						$L_{\text{lim}} = 0.25 L^*$						$L_{\text{lim}} = 0.5 L^*$						$L_{\text{lim}} = L^*$					
			Physical			Scaled by R_{vir}			Physical			Scaled by R_{vir}			Physical			Scaled by R_{vir}			Physical			Scaled by R_{vir}		
			L	D	D/R _{vir}	L	D	D/R _{vir}	L	D	D/R _{vir}	L	D	D/R _{vir}	L	D	D/R _{vir}	L	D	D/R _{vir}	L	D	D/R _{vir}	L	D	D/R _{vir}
PHL 1811	0.07777	n	0.076	0.235	0.246	2.72	0.695	0.542	3.23	3.01	0.695	0.542	3.23	3.01	0.695	0.542	3.23	3.01	0.695	0.542	3.23	3.01	1.29	0.790	3.23	3.01
PHL 1811	0.12060	n	0.169	1.23	0.169	12.2
PHL 1811	0.13229	y	0.645	0.228	0.645	1.45	0.645	0.228	0.645	1.45	0.645	0.228	0.645	1.45	0.645	0.228	0.645	1.45	0.645	0.228	0.645	1.45	2.65	2.39	2.65	9.53
PHL 1811	0.13547	y	0.150	0.519	0.150	5.30	0.333	1.02	1.14	6.04	0.333	1.02	1.14	6.04	0.333	1.02	1.14	6.04	0.333	1.02	1.14	6.04	1.14	1.15	1.14	6.04
PKS 0405-123	0.09180	y	0.010	0.135	0.010	2.37	0.345	0.449	0.345	3.51	0.345	0.449	0.345	3.51	0.345	0.449	0.345	3.51	0.345	0.449	0.345	3.51
PKS 0405-123	0.09655	y	0.739	0.270	0.739	1.65	0.739	0.270	0.739	1.65	0.739	0.270	0.739	1.65	0.739	0.270	0.739	1.65	0.739	0.270	0.739	1.65	1.93	0.934	1.93	4.15
PKS 2005-489	0.01695	y	0.002	0.255	1.15	3.30
PKS 2005-489	0.06499	y	0.024	0.529	15.2	5.52
Q 1230+0115	0.07807	y	0.175	0.054	0.175	0.529	0.652	0.528	0.652	3.36	0.652	0.528	0.652	3.36	0.652	0.528	0.652	3.36	0.652	0.528	0.652	3.36	1.12	1.52	2.40	7.92
SBS 1122+594	0.14315	n	0.599	0.529	0.599	3.46
SBS 1122+594	0.15545	y	0.577	0.115	0.577	0.762
TON 580	0.13396	n	0.456	0.859	0.456	6.14	0.456	0.859	0.456	6.14	0.456	0.859	0.456	6.14	0.456	0.859	0.456	6.14	0.456	0.859	0.456	6.14	1.05	1.67	2.16	7.80

PREVIOUS METALS INTO THE IGM

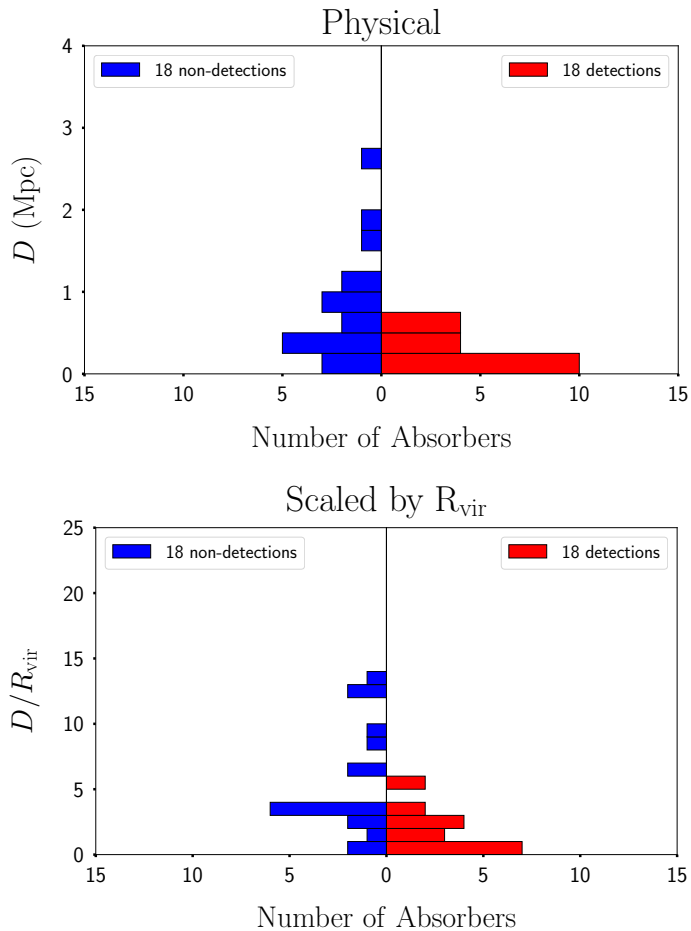


Figure 1. Histograms of O VI nearest galaxy distances in Mpc (*top*) and scaled nearest galaxy distances in units of R_{vir} (*bottom*). The red bars to the right represent the O VI detections, and the blue bars to the left are non-detections. No galaxy luminosity limit was applied for these data, thus utilizing all of the galaxy redshift data we have available (i.e., columns 4-7 of Table 3).

3. THE SPREAD OF O VI AROUND LOW- Z GALAXIES

The most straightforward way to examine the spread of O VI from galaxies is through Figure 1 which shows the 18 O VI detections and 18 O VI non-detections in double-sided histograms. The top histogram shows that O VI spreads no more than the 750 kpc bin from the nearest galaxy; the specific largest value is 620 kpc. The median luminosity of the galaxy physically nearest to metal-enriched IGM absorbers is $0.61 L^*$; this median becomes $0.66 L^*$ when considering galaxies nearest to absorbers in units of R_{vir} . Due to the large variation in nearest galaxy luminosities and thus virial radii, the metal spread extends to as much as $5 R_{\text{vir}}$ in some cases, leaving little doubt that the most remote absorbers are unbound gravitationally from the nearest galaxy.

Using the “matched” subsamples of 10 O VI detections and 10 non-detections, the impact parameter distribution shown in Figure 1 remains largely unchanged; i.e., the O VI absorbers are closer to their associated galaxy, but the statistical difference is smaller (p -value = 0.27). The lower probability ($\approx 70\%$) of being drawn from different parent populations is due primarily to the much smaller sample size of ten pairs only. This statement was verified through the fiat of creating new subsamples by counting each detection and non-detection twice. This reduced the Anderson-Darling p -value from 0.27 to 0.05. Similar to the full samples, however, the matched samples contain no O VI absorbers beyond $\rho = 0.6$ Mpc while nearly 50% of the O VI non-detections are at $\rho > 0.6$ Mpc, including one O VI-deficient absorber at $\rho > 2$ Mpc.

To determine the maximum spread of metals more robustly, we show cumulative distribution functions (CDFs) in Figure 2 for three different L_{lim} cuts in our galaxy survey where the sampling is complete to $\geq 90\%$. Absorbers are included in each luminosity bin **only if** the galaxy survey is complete at or below L_{lim} .

The Anderson-Darling test was then used to determine the likelihood these two distributions were randomly drawn from the same parent population. For the $L \geq L^*$ subsample, there is virtually no difference between the distributions of galaxies nearest to O VI detections and non-detections. The greatest contrast (p -value = 0.025) between the detections and non-detections is for the $L \geq 0.5 L^*$ subsample, for which the median distances to O VI detections (0.38 Mpc and $2.22 R_{\text{vir}}$) are considerably smaller than those for non-detections (0.70 Mpc and $3.51 R_{\text{vir}}$).

When applying these same galaxy survey constraints to the N_{HI} matched samples of absorbers, the sizes of O VI detections and non-detections decrease to single digits for each luminosity cut. Similar to the full samples, the impact parameters to O VI detections are systematically smaller than non-detections. The reduced sample sizes, however, render any statistical tests for differences quite uncertain; e.g., the $L > 0.5 L^*$ samples differ only with a p -value = 0.24. While the results from the matched samples support the inference that O VI detections are more closely associated with galaxies than non-detections, they do not do so strongly. Therefore, we now turn our attention to those tests which use only the full sample of O VI detections.

By using only those 11 absorbers in the full sample of O VI detections, whose surroundings were surveyed to at least $0.25 L^*$, we inspected the luminosities of the physically nearest galaxies: there are four $L < 0.5 L^*$ galaxies, seven $0.5 L^* \leq L < L^*$ galaxies, and zero $L \geq$

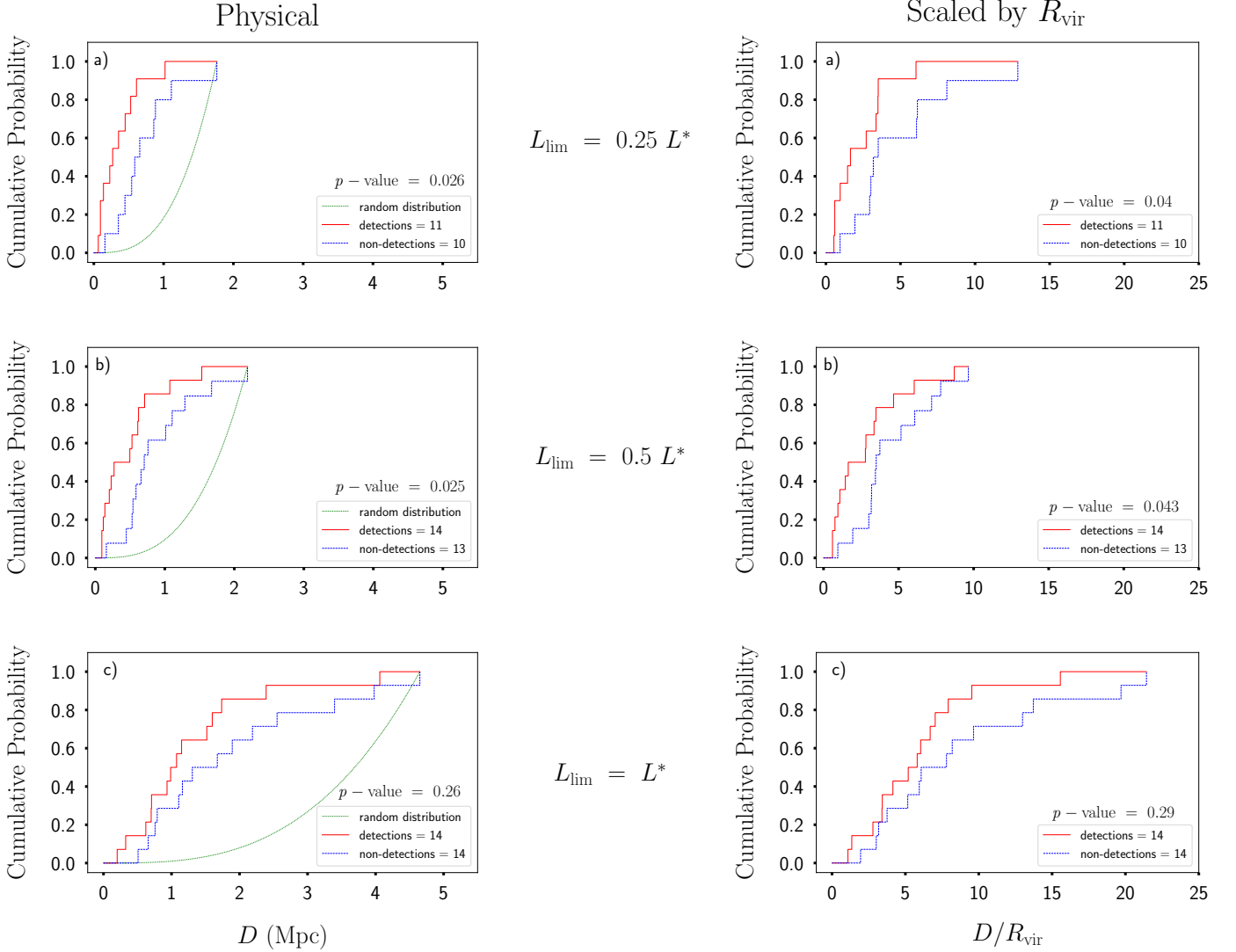


Figure 2. Cumulative distribution functions of O VI nearest galaxy distances (*left*) and distances scaled by R_{vir} (*right*). The solid red lines represent O VI detections, the dashed blue lines are O VI non-detections, and the dotted green lines represent a random distribution of galaxies within a similar volume. The different panels (a-c) show the limiting luminosities of $0.25 L^*$, $0.5 L^*$, and $1 L^*$. All panels show a p -value found by the Anderson-Darling test, used to compare the distributions of O VI detections to non-detections given the full samples of absorbers.

L^* galaxies. This is intriguing evidence that the primary contributor to spreading metals into the CGM/IGM are galaxies somewhat fainter than L^* , similar to the Milky Way and M33.

To better compare our results for different L_{lim} , we scale the absorber-galaxy distance by the mean distance between galaxies of equal or greater luminosity ($\langle D_{\text{int}} \rangle$), given by the inverse cube root of the integral galaxy luminosity function. The SDSS luminosity function of [Montero-Dorta & Prada \(2009\)](#) with K -corrections from [Chilingarian, Melchior, & Zolotukhin \(2010\)](#) and [Chilingarian & Zolotukhin \(2012\)](#) were used to find values of: $\langle D_{\text{int}} \rangle = 5.96, 7.45, \text{ and } 10.4$ Mpc for $L_{\text{lim}} = 0.25, 0.5, \text{ and } 1 L^*$, respectively.

[Figure 3](#) compares the CDFs of the O VI detections for the three different L_{lim} subsamples. The median value of $D/\langle D_{\text{int}} \rangle$ for the $L_{\text{lim}} = 0.5 L^*$ subsample finds that these galaxies are ~ 20 times closer to absorbers than they are to other $L \geq 0.5 L^*$ galaxies. Clearly, O VI absorbers are tightly correlated with sub- L^* galaxies.

4. SUMMARY OF RESULTS AND DISCUSSION

Based on high-S/N, high-resolution FUV spectroscopy for samples of low- z O VI absorption-line detections and non-detections, we find that O VI is not detected beyond a physical distance of ~ 0.6 Mpc, or $\sim 5 R_{\text{vir}}$ from the nearest galaxy. These results are in good agreement with those found by [Stocke et al. \(2006\)](#), who reported a spread of O VI to a maximum physical distance of

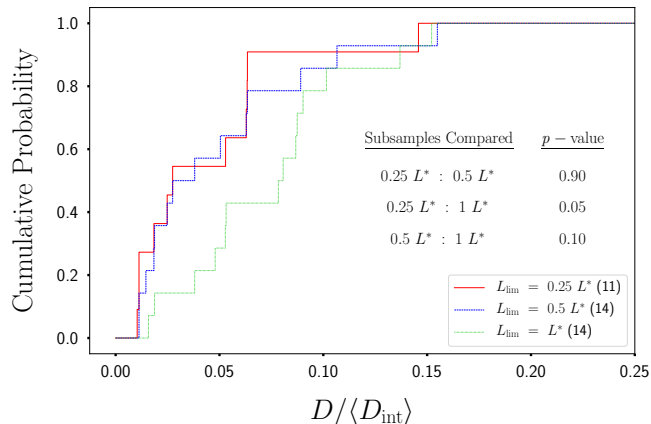


Figure 3. Cumulative distribution functions of O VI nearest galaxy distances scaled by the mean distances between galaxies of similar or greater luminosity. The red, blue, and green lines show the results for $L_{\text{lim}} = 0.25$, 0.5 , and $1 L^*$, respectively. The Anderson-Darling p -values comparing the subsamples are shown in the figure.

~ 800 kpc, or 3.5 - $5 R_{\text{vir}}$ from $L \geq L^*$ galaxies. More recently, Johnson, Chen, & Mulchaey (2015) reported O VI detections at 1 - $3 R_{\text{vir}}$ around galaxies of luminosities $L > 0.1 L^*$ at $z < 0.4$. Also, the correlation lengths found here are similar to those found by Finn et al. (2016) in a large, statistical study of low- z O VI absorbers. Since these other recent studies use *HST*/*COS* FUV spectra of comparable or lesser S/N as the present study, these conclusions are all limited to modest metallicity gas (a median level of $Z \sim 0.1 Z_{\odot}$ is suggested for this sample by the results of Savage et al. 2014); lower metallicity gas may be more pervasive in the IGM at both low- and high- z (e.g., Aguirre, Schaye, & Theuns 2002) than as measured here. Despite significant differences between the CDFs of O VI detections and non-detections, many O VI non-detections are found at comparable impact parameters to the detections as shown in Figure 2 and Figure 3. We interpret this result as an indication of rather pristine gas falling onto galaxies from the IGM (see also Stocke et al. 2013).

By creating subsamples, defined by L_{lim} , we find evidence that O VI absorbers are more tightly correlated with $L < L^*$ galaxies than $L \geq L^*$ galaxies. Specifically, using only those absorbers with galaxy surveys complete $0.25 L^*$, we find that **all** of O VI absorbers studied have physically nearest galaxies in the $0.25 L^* < L < L^*$ range. This result suggests that the majority of metals expelled into the CGM/IGM originate in sub- L^* galaxies ($0.25 L^* < L < L^*$ for the purposes of this study).

The hypothesis that O VI absorbers are associated primarily with low-luminosity galaxies was originally proposed by Tumlinson & Fang (2005) based on the dN/dz of O VI absorption systems, a hypothesis that was sup-

ported by our first galaxy-absorber study (Stocke et al. 2006). Later, Prochaska et al. (2011) made a similar suggestion based on their galaxy survey work, specifically identifying sub- L^* galaxies as the primary associated galaxies for low- z Ly α and metal-line systems. More recently, a very deep galaxy survey ($L \geq 0.01 L^*$) by Burchett et al. (2016) found C IV absorption associated primarily with galaxies at $L \geq 0.3 L^*$. Although the present galaxy survey is not as deep as that used by Burchett et al. (2016), our results are consistent with the intriguing speculation that CGM/IGM metals come primarily from sub- L^* galaxies. The combination of the Burchett et al. (2016) result, which suggests a lower luminosity bound of $L \geq 0.3 L^*$, and the present study, which suggests an upper bound of $L \leq L^*$, limits the bulk of the metals ejected to a source population in the sub- L^* regime.

Theoretical studies suggest $L > L^*$ galaxies are too massive to allow metal-enriched gas to easily escape beyond R_{vir} while true dwarfs may eject too little gas *in toto* to be major contributors to CGM/IGM “metal pollution”. Since the sub- L^* galaxy population possesses bulk metallicities of a few tenths solar values (Tremonti et al. 2004), which is comparable to the absorber metallicities found for photo-ionized CGM absorbers (Stocke et al. 2013; Werk et al. 2014; Keeney et al. 2017), outflows escaping from these modest mass galaxies would not require significant dilution by more pristine gas to be observed as low- z CGM metal-line systems.

This study shows that O VI is not spread beyond distances ~ 0.6 Mpc, comparable to or less than the size of a small galaxy group ($R_{\text{vir}} \approx 1$ Mpc for a group halo of $10^{13.5} M_{\odot}$) or width of a large-scale structure filament. Specifically, this distance is significantly greater than the virial radius of even a single $10 L^*$ galaxy while being comparable to the virial radius of a small group of galaxies with $L \sim 2 L^*$.

The current sample includes absorbers associated with 8 well-studied galaxy groups (5 O VI detections and 3 non-detections) with total luminosities of 4 - $55 L^*$ (estimated halo masses of $10^{13.5-15} M_{\odot}$ Stocke et al. 2013). While a few O VI detections occur in rather sparse regions (e.g., PKS 0405-123/0.09180) that are in at best very poor groups of galaxies, most of the absorbers in this survey have galaxy densities comparable to the 8 for which detailed group membership analyses have been done. The absence of metal-bearing absorbers at $\rho > 0.6$ Mpc, even from quite low luminosity galaxies, argues that galactic winds do not stream freely away from individual galaxies and groups. For example, even a galactic wind speed of 200 km s^{-1} will carry metals to ~ 0.6 Mpc in only 3 billion years if unimpeded by gravity

or mass-loading. Other studies (Penton, Stocke, & Shull 2004; Stocke et al. 2007) have set only upper limits, of a few percent solar values, on metallicities of absorbing gas found several Mpc from the nearest galaxy in “voids”. This result and the current study support the hypothesis that most or all of the metals produced in galaxies remain within the confines of the galaxy group in which the source galaxy is a member. Because more isolated galaxies are poorly represented in this study, we cannot draw any firm conclusions about the spread of metals from those systems.

In conclusion, relatively pristine ($Z < 0.1 Z_{\odot}$) gas can be accreted by a galaxy group, and the metal-enriched gas expelled by the member galaxies does not appear to be transported to distances beyond the group radius. While luminosity function studies of galaxy groups find many more sub- L^* galaxies than $L > L^*$ galaxies (i.e., groups have luminosity functions approximately given by Schechter functions), differences in the relative numbers of sub- L^* galaxies in groups are observed (Zabludoff & Mulchaey 2000) and could create different metallicity evolution histories between groups if all of their metals are retained inside the group. This may contribute to the substantial width observed in the mass-metallicity relationship (Tremonti et al. 2004).

It is likely that both collisionally-ionized (CIE) and photo-ionized (PIE) OVI absorbers are present in this sample. Based on an unbiased O VI sample from Savage et al. (2014), $\sim 1/3$ of all O VI absorbers at the $N_{\text{O VI}}$ levels investigated here have inferred $T \geq 10^5$ K. Some of these CIE O VI absorbers likely arise in warm-hot gas which may be associated with entire galaxy groups (Stocke et al. 2014). However, it is challenging to ascribe any individual absorber unambiguously to either an individual galaxy or to the entire group to which it belongs, since most star-forming galaxies are members of small groups (Tully et al. 2009) and almost all “passive” galaxies are members of rich groups or clusters (Dressler et al. 1997). We have not attempted to make that distinction here but leave this more challenging question to on-going and future investigations which include our own HST study of H I and O VI-absorbing gas associated with rich groups of galaxies (see e.g., Stocke et al. 2017).

Facilities: AAT (AAΩ), Blanco (HYDRA, MO-SAIC), FUSE, HST (COS), MMT (Hectospec), Sloan, WIYN (HYDRA), WIYN:0.9m (MOSAIC)

This work was supported by NASA grants NNX08AC146 and NAS5-98043 to the University of Colorado at Boulder for the *HST*/COS project. CTP, JTS, and BAK gratefully acknowledge support from NSF grant AST1109117.

REFERENCES

- Aguirre, A., Schaye, J., & Theuns, T. 2002, *ApJ*, 576, 1
- Alam, S., Albareti, F. D., Allende Prieto, C., et al. 2015, *ApJS*, 219, 12
- Binney, J., & Tremaine, S. 1987, *Galactic dynamics*
- Bordoloi, R., Fox, A. J., Lockman, F. J., et al. 2017, *ApJ*, 834, 191
- Burchett, J. N., Tripp, T. M., Bordoloi, R., et al. 2016, *ApJ*, 832, 124
- Cen, R., & Ostriker, J. P. 1999, *ApJ*, 514, 1
- Chen, H.-W., Lanzetta, K. M., Webb, J. K., & Barcons, X. 1998, *ApJ*, 498, 77
- Chilingarian, I. V., Melchior, A.-L., & Zolotukhin, I. Y. 2010, *MNRAS*, 405, 1409
- Chilingarian, I. V., & Zolotukhin, I. Y. 2012, *MNRAS*, 419, 1727
- Colless, M., Dalton, G., Maddox, S., et al. 2007, *VizieR Online Data Catalog*, 7250
- Côté, B., Martel, H., Drissen, L., & Robert, C. 2012, *MNRAS*, 421, 847
- Danforth, C. W., Keeney, B. A., Tilton, E. M., et al. 2016, *ApJ*, 817, 111
- Davé, R., Finlator, K., & Oppenheimer, B. D., 2011, *MNRAS*, 416, 1354
- Davé, R., Hernquist, L., Katz, N., & Weinberg, D. H. 1999, *ApJ*, 511, 521
- Dressler, A., Oemler, A., Jr., Couch, W. J., et al. 1997, *ApJ*, 490, 577
- Ferland, G. J., Korista, K. T., Verner, D. A., et al. 1998, *PASP*, 110, 761
- Finn, C. W., Morris, S. L., Tejos, N., et al. 2016, *MNRAS*, 460, 590
- Green, J. C., Froning, C. S., Osterman, S., et al. 2012, *ApJ*, 744, 60
- Hayward, C. C., & Hopkins, P. F. 2017, *MNRAS*, 465, 1682
- Hopkins, P. F., Torrey, P., Faucher-Giguère, C.-A., Quataert, E., & Murray, N. 2016, *MNRAS*, 458, 816
- Johnson, S. D., Chen, H.-W., & Mulchaey, J. S. 2015, *MNRAS*, 449, 3263
- Jones, D. H., Read, M. A., Saunders, W., et al. 2009, *MNRAS*, 399, 683
- Keeney, B. A., Danforth, C. W., Stocke, J. T., et al. 2006, *ApJ*, 646, 951
- Keeney, B. A., Stocke, J. T., Danforth, C. W., et al. 2017, *ApJS*, 230, 6
- Lanzetta, K. M., Bowen, D. V., Tytler, D., & Webb, J. K. 1995, *ApJ*, 442, 538
- Montero-Dorta, A. D., & Prada, F. 2009, *MNRAS*, 399, 1106
- Muratov, A. L., Kereš, D., Faucher-Giguère, C.-A., et al. 2015, *MNRAS*, 454, 2691
- . 2017, *MNRAS*, 468, 4170
- Oppenheimer, B. D., Davé, R., Katz, N., Kollmeier, J. A., & Weinberg, D. H. 2012, *MNRAS*, 420, 829
- Pagel, B. E. J. 2009, *Nucleosynthesis and Chemical Evolution of Galaxies*
- Penton, S. V., Stocke, J. T., & Shull, J. M. 2004, *ApJS*, 152, 29
- Prochaska, J. X., Weiner, B., Chen, H.-W., Mulchaey, J., & Cooksey, K. 2011, *ApJ*, 740, 91
- Prochaska, J. X., Werk, J. K., Worseck, G., et al. 2017, *ApJ*, 837, 169
- Savage, B. D., Kim, T.-S., Wakker, B. P., et al. 2014, *ApJS*, 212, 8
- Shull, J. M. 2014, *ApJ*, 784, 142
- Stocke, J. T., Danforth, C. W., Shull, J. M., Penton, S. V., & Giroux, M. L. 2007, *ApJ*, 671, 146
- Stocke, J. T., Keeney, B. A., Danforth, C. W., et al. 2013, *ApJ*, 763, 148
- Stocke, J. T., Penton, S. V., Danforth, C. W., et al. 2006, *ApJ*, 641, 217
- Stocke, J. T., Keeney, B. A., Danforth, C. W., et al. 2014, *ApJ*, 791, 128
- Stocke, J. T., Keeney, B. A., Danforth, C. W., et al. 2017, *ApJ*, 838, 37
- Steidel, C. C., Erb, D. K., Shapley, A. E., et al. 2010, *ApJ*, 717, 289
- Tilton, E. M., Danforth, C. W., Shull, J. M., et al. 2012, *ApJ*, 759, 112
- Tremonti, C. A., Heckman, T. M., Kauffmann, G., et al. 2004, *ApJ*, 613, 898
- Tully, B. R., Rizzi, L., Shaya, E. J., et al. 2009, *AJ*, 138, 323
- Tumlinson, J., & Fang, T. 2005, *ApJL*, 623, L97
- Tumlinson, J., Thom, C., Werk, J. K., et al. 2011, *Science*, 334, 948
- Veilleux, S., Cecil, G., & Bland-Hawthorn, J. 2005, *ARA&A*, 43, 769
- Werk, J. K., Prochaska, J. X., Tumlinson, J., et al. 2014, *ApJ*, 792, 8
- Zabludoff, A. I., & Mulchaey, J. S. 2000, *ApJ*, 539, 136